Fermi National Accelerator Laboratory

FN-511-Rev.
[SSC-212]

Ground-Motion Effects on the SSC

King-Yuen Ng
Fermi National Accelerator Laboratory
P.O. Box 500
Batavia, Illinois 60510

and

Jack Peterson
Superconducting Super Collider Laboratory
8901 Autobahn
Dallas, Texas 75237

December 1989

Operated by Universities Research Association Inc. under contract with the United States Department of Energy

SSC-212
FN-511

GROUND-MOTION EFFECTS ON THE SSC

King-Yuen Ng

Fermi National Accelerator Laboratory, Batavia, IL 60510

and

Jack Peterson

SSC Laboratory, 8901 Autobahn, Dallas, TX 75237

(November 1989)

(Revised Deccember 1989)

Due to a bug in one of the computer codes, parts of Sections 4.2, 4.3, 4.4, and Figures 7, 8, 9 have been revised.

1. INTRODUCTION

Ground motion at the one-micron level can seriously degrade the collider performance. Motion of the quadrupole magnets is the main concern. Because of the high magnetic gradients in the quadrupoles, a small horizontal or vertical motion can result in a significant change in the central (closed) orbit in each of the two rings. Furthermore, for a proton-proton collider, the orbit changes in the two rings are different because the quadrupoles are arranged asymmetrically in the two rings—i.e., a focusing quadrupole in one ring always occurs with a defocusing quadrupole in the other ring. As a consequence, at each of the four collision points, the changes in the two closed orbits due to ground motion are likely to be different, thus causing the two beam centers to miss each other with a consequent reduction in luminosity.[1]

In this report we examine these effects quantitatively for plane waves, for spreading waves from point sources, and for waves from a distribution of point sources, such as a train, but in an ideal, uniform, and semi-infinite model of the SSC site. More data on ground motion and attenuation effects at the actual SSC site are certainly needed.

2. BACKGROUND THEORY

2.1 Closed-orbit effects

The effect of shifting in a transverse direction y one quadrupole magnet in an accelerator ring is to perturb the closed orbit by a stationary wave $y(s)$ having the local betatron wavelength everywhere around the ring and a constant normalized amplitude (see Figure 1):

$$y(s) = \frac{\Delta y \sqrt{\beta_Q \beta(s)}}{2f \sin \pi\nu} \cos(\phi - \pi\nu) \tag{1}$$

where Δy is the transverse shift, f the quadrupole focal length (positive for F-quads and negative for D-quads), β_Q the value of the y-betatron function at the

displaced quad, $\beta(s)$ the y-betatron function at point s, ϕ the y-betatron phase from the displaced quad, and ν the betatron tune in the y-plane. Thus, one must consider the motion of *all* the quadrupoles in the ring, not just those near the interaction points. Since Eq. (1) points out that the wavelength of the closed-orbit disturbance produced by the shift of one quadrupole magnet is just the betatron wavelength of the accelerator ring, we should be warned at this point to expect notable effects at ground-motion wavelengths that are harmonically related to the accelerator wavelength.

To obtain the effect due to displacements of all the quadrupoles in the ring, Eq. (1) is applied to each quadrupole and the results summed. Thus for any static arrangement of Δy around the two rings, the shift in the closed orbit in each can be evaluated at any desired point. The difference in the two closed orbits at each of the four interaction points then is the amount by which the two beam centers will miss each other. If this difference is larger than, say, one-tenth of the beam dimensions at the crossing, the resulting drop in luminosity will call for compensation or reduction of these closed-orbit shifts. The nominal beam dimensions (r.m.s. radii) at the collision points are $\sigma_t = 4.8$ microns in the low-beta crossings and 22 microns in the medium-beta crossings, so that we shall be concerned with closed-orbit differences in the fractional-micron range in the low-beta crossings and in the 2-micron range in the medium-beta crossings.

In principle, this closed-orbit problem is, of course, time dependent, so that at some frequency the static approximation will be inadequate. However, it will develop that the principal groundwave frequencies of interest are in the 1 to 10 Hz, whereas the beam in the SSC circulates at 3.6 kHz. Thus, the beam effects are essentially adiabatic so that the static approximation should be valid.

Shifting a quadrupole in the longitudinal direction has no effect at all on a closed orbit that traverses the center of that quadrupole with zero slope. Also it is easily shown for closed orbits that are not centered in the SSC quadrupoles that the effects of a longitudinal shift is several orders of magnitude smaller than

that of a similar shift in the transverse direction. For this reason we can neglect longitudinal motion of the quadrupoles.

Shifting a pure dipole in the transverse direction has no effect in a beam trajectory. Only the end fields and the harmonic multipole fields at the trajectory can in principle be affected. Since the end fields are mainly equivalent to quadrupoles that are much, much weaker than the lattice quadrupoles, the end-field effects also can be neglected. Next, consider the perturbation due to shifting a multipole in the body of the dipole. As an example, a 1 "unit" quadrupole error in each of the dipoles of a half cell forms a total quadrupole strength that is less than 1% of the lattice quadrupole strength in that half cell. Similar considerations of the higher multipoles of the strengths expected show that they too can be neglected.

2.2 Uniform Ring Model

Rossbach[2] has calculated the closed-orbit shifts produced by a plane ground wave of wavelength λ and incident angle θ_w in a circular ring with a uniform FODO lattice of N cells, with a phase shift of μ per cell. Even for this relatively simple case a complicated expression is needed to describe the variation of the closed-orbit amplitude y_c with λ and θ_w:

$$y_c = \mathrm{Re}\left[A \sum_{p=-\infty}^{+\infty} i^p J_p\left(\frac{C}{\lambda}\right) C_p\right] \tag{2}$$

with

$$C_p = \frac{(-1)^{p-1}}{\sin(\pi p/N - \mu/2)} \left\{\sqrt{\hat{\beta}} \cos\left[p\left(\pi \frac{N+1}{N} - \theta_w\right) - \frac{\mu}{2}\right] - \sqrt{\hat{\beta}}\, \cos p(\pi - \theta_w)\right\}$$

J_p = Bessel function of the first kind and order p

C = ring circumference

$A = \frac{\sqrt{\beta_0}}{2} \frac{\hat{y}}{f} e^{i(\omega t + \phi_0)}$

β_0 = betatron function at the reference point

$\hat{y}$ = peak ground wave amplitude

f = quadrupole focal length

ϕ_0 = phase of ground wave relative to the ring center

Of the infinite sum the only important terms are those for which the denominator in C_p produces a resonance. That is, only the important terms are those for which the integer p obeys the relation

$$|p| = |m|\, N \pm \nu_y \tag{3}$$

where m is some integer and ν_y the betatron tune. The lowest-order resonance values of p are:

$$|p_{\rm res}|_1 = [\nu_y]$$
$$|p_{\rm res}|_2 = N - [\nu_y]$$
$$|p_{\rm res}|_3 = N + [\nu_y]$$

where $[\nu_y]$ is the integer nearest to ν_y. For a 90° lattice $N = 4[\nu_y]$. Thus, we have two important results: (1) that the *wavelength* of the ground wave is its important parameter (not its frequency) and (2) that the *largest* wavelength of importance is equal to the betatron wavelength.

Figure 2 is a plot from Rossbach's article showing the variation of closed-orbit amplitude with the number of ground-wavelengths per circumference (C/λ) and also with respect to the direction of propagation of the ground wave for the case of the European Synchrotron Radiation Facility, for which $C = 850$ m, $\nu_y = 19.2$, and $N = 80$. The plot against C/λ shows prominent maxima at $[\nu_y]$, $N - [\nu_y]$, and

$N + [\nu_y]$ in agreement with Eq. (3). The minor peaks are the peaks in the Bessel functions $J_{19}(C/\lambda)$ and $J_{61}(C/\lambda)$. Note the vanishing closed-orbit response for the ground wavelength greater than the betatron wavelength ($C/\lambda < 19$).

The lower curve in Figure 2 shows the extremely complicated angular variation for the (arbitrary) case of the ground wavelength equal to about one-third of the betatron wavelength ($C/\lambda = 62$). These complications are understandable in terms of Eq. (2), but we should be prepared to expect even more complicated behavior in the case of the SSC because of its larger size and betatron tune and because of the irregular structure due to interaction straight sections and their special optics.

2.3 Ground Waves

There are several types of wave motion that can propagate through the earth.[3,4] Let us first consider the idealized model of the earth as a homogeneous, isotropic, elastic, semi-infinite medium being excited by a point source vibrating vertically on the surface. Three types of waves can be produced. For completeness, their derivations are included in the Appendix. Here, we just list some of their properties.

1. A spherical compression wave ("p-wave") propagating at the highest wave velocity v_p equal to $\sqrt{C_{11}/\rho}$, where C_{11} is the compressional elastic constant of the medium and ρ its density.

2. A spherical shear wave ("s-wave") propagating at a lower velocity v_s equal to $\sqrt{C_{44}/\rho}$, where C_{44} is the shear elastic constant.

These two spherical waves are referred to as the "body" waves. In the "far zone" (at distances greater than a wavelength or so) the amplitude variation of each is simply of the form

$$a(R,\theta) \;=\; \frac{A\,R_0}{R}\,f(\theta)\;, \tag{4}$$

where A is the amplitude at reference radius R_0, and $f(\theta)$ is the dependence on

the polar angle.

3. The third type of wave is a ground wave (or "Rayleigh" wave) that propagates at a speed v_R that is somewhat less than the speed v_s of the shear body wave. The Rayleigh wave has both compressional and vertical shear components. In such a wave a particle of earth is moved along an elliptical path, both up and down and forward and back, like (but not the same as) a drop of water in a surface wave in the ocean. The distribution is cylindrical—i.e., uniform in azimuthal angle, as $R^{-\frac{1}{2}}$ in radius, and exponentially decreasing in depth:

$$a(R,z) = A\left(\frac{R_0}{R}\right)^{\frac{1}{2}}\left(a_1 e^{-b_1 z} + a_2 e^{-b_2 z}\right) , \tag{5}$$

where a_1, a_2, b_1 and b_2 are constants depending on C_{11} and C_{44}, the compressional and shear elastic constants of the medium. The e-fold distances $1/b_1$ and $1/b_2$ are both of the order of magnitude of the p-wave wavelength. Note that the ground wave falls off more slowly than the body waves with radius from the source. For a case considered by Miller and Pursey[4] with Poisson's ratio $\frac{1}{4}$, it turned out that about two-thirds of the energy propagating from a point source went out in the surface wave.

A second type of surface waves, called "Love waves," can occur under certain conditions. Horizontally polarized shear waves can propagate as a trapped mode in a surface layer, provided that the shear wave velocity in that medium is lower than that in the underlying medium. The velocity of the Love wave, like that of the Rayleigh surface wave, is somewhat less than that of the body shear wave in the underlying medium. We should note that the Love wave can be produced by a source on the surface that is vibrating in the horizontal plane.

The wave propagation described by Eqs. (4) and (5) does not include attenuation effects. The total wave energy is the same at all distances. To include energy dissipation these equations must include factors of $e^{-\alpha R}$ and/or $e^{-\alpha z}$. The

attenuation constant α can normally be expressed as

$$\alpha = \frac{\pi f}{Qv} \ , \tag{6}$$

where f is the frequency of the wave, v its velocity, and Q the quality factor. Nelson[3] states that for some soil materials the Q is almost independent of frequency (so that α is roughly linear with frequency), but that for some other soil materials α is approximately independent of frequency between 10 and 30 Hz. As we shall see, it will be important to understand the attenuation effects at the SSC site.

Another important complication is the layered structure of a site. At interfaces between materials of different elastic properties and densities, not only are reflected and transmitted waves produced but also mode conversion can occur. That is, an incident compression wave, e.g., can produce reflected and transmitted shear waves, and vice versa. Thus, in a real site the description of ground wave transmission can be exceedingly complicated.

3. SOURCES OF GROUND MOTION

Fischer and Morton[5] surveyed sources of ground motion that might affect the operation of the SSC. They considered both natural sources and cultural sources.

Of the natural sources of ground motion that they considered—namely, earth tides, earthquakes, and ambient microseismic noise, only the ambient microseismic noise had components that could be of serious concern to SSC operation. Figure 3, from Aki and Richards,[5,6] shows the long-term average of the power spectral density in microseismic noise for "noisy" and "quiet" sites. The ground motion amplitude at the peak in the "noisy" site spectrum at about 0.2 Hertz is about 1 micron. Such an amplitude is of concern to the SSC if the corresponding ground wavelength is 900 meters or less, corresponding to a shear-wave speed of

180 meters/sec or less. Since the p-wave speed in Austin chalk, the main component in the Texas site, is probably 3 km/sec or slightly less, it is likely that microseismic noise will not seriously affect SSC operation.

Cultural sources of ground motion, on the other hand, can be of concern to the SSC. Figures 4a and 4b show the measured amplitude of ground motion at 100 feet from a train near the proposed location of the SSC tunnel both as a function of time and in terms of its frequency spectrum. Figures 4c and 4d similarly show the ground motion at about 6 miles from a blast in a limestone quarry located a few miles from the SSC ring. Both figures show ground motion amplitude up to about 2 microns. We want to determine whether such ground motion will require dynamic feedback or other counter measures. Fischer and Morton[5] estimated that the tolerance without feedback was about 0.4 micron in the frequency range 3 to 20 Hertz.

4. CALCULATION OF GROUND-WAVE EFFECTS ON THE SSC

The effects on the closed orbits in the two rings of the SSC due to motion of the quadrupole magnets caused by ground waves were calculated for a variety of cases:

a. vertical shear plane waves for many wavelengths and directions of incidence, but with no attenuation.

b. body and surface waves from a vertically vibrating point source, at many locations in the region of the SSC and over a spectrum of frequencies, but with no attenuation.

c. body and surface waves from a battery of point sources simulating a train at several locations, but with no attenuation.

d. body and surface waves from point sources including attenuation.

The complete SSC lattice[7] was modeled in collision optics. The position of every quadrupole was modulated by the ground waves. The components of the

motion in the vertical and horizontal directions were separately applied to calculate the vertical and horizontal closed-orbit shifts at the four collision points (two low-beta and two medium-beta) for each of the two collider rings. The difference between the two closed-orbit shifts at each of the four points was taken, and r.m.s. average over time and phase was calculated. Two modes of computation were used with complete agreement; the closed-orbits were calculated for a few cases using the TEAPOT particle-tracking code but the bulk of the results were obtained by the much faster method of applying the analytic formula [Eq. (1)] to each quadrupole in each ring for each ground-wave situation and summing the results at each of the four beam crossings.

In Eq. (1), the transverse ground displacement Δy carries a time variation $\exp(\omega t - \phi_0)$, where $\omega/2\pi$ is the frequency and ϕ_0 is a phase relative to, say, the center the of collider. If a particle-tracking code is used, computation has to be done for *many* ϕ_0's and an average is then taken. However, the ground displacement Δy would be the same for the two quads at the same location in the two rings. Therefore, the actual computation of the difference in the two closed orbits using Eq. (1), this exponential factor can be factored out and discarded. The r.m.s. closed-orbit difference at s will just be the absolute value of the difference in the two closed-orbit shifts $y(s)$ summed over all quadrupoles and divided by $\sqrt{2}$. One can visualize how much computer time can be saved when the analytic formula is used. The deviations from tracking results are negligible.

4.1 Plane Ground Waves

The separations of the two closed orbits at the collision points due to vertically polarized plane shear waves are illustrated in Figures 5 and 6. No attenuation of the waves was assumed. Figure 5 shows the variation with ground wavelength for two directions of propagation at a low-beta crossing and at a medium-beta crossing caused by waves having one micron displacement. Figures 5a–b shows the variation for the case of waves incident at 0 degrees (waves incident in the east/west direction on a collider aligned with its long axis in the north/south

direction).

Note: (1) the strong response at a ground wavelength of about 880 meters, which is close to the *average* betatron wavelength ($2\pi R/\nu_y = 83,631/95.2 = 878.5$ m), (2) the zero response at wavelengths longer than 880 meters, and (3) the regular variation at shorter wavelengths. All three features are in agreement with Rossbach's uniform-ring model[2] illustrated in Figure 2. In fact, the 880 m wavelength is exactly $2\pi R/[\nu_y]$, where $[\nu_y] = 90$ is the integer nearest to ν_y.

Note that ground wave amplitudes of 1 micron can produce orbit separations up to 3 microns (60% of σ_y) at the low-beta crossings and 9 microns (40% of σ_y) at the medium-beta crossings.

Figures 5c–5d show the corresponding response for plane waves traveling along the northeast/southwest direction. The strong peak at the average betatron wavelength is again present, but for waves in this direction, where the SSC ring presents less symmetry, there is a small response at ground wavelengths *longer* than the average betatron wavelength, and the response at shorter wavelengths is very irregular.

The SSC ring has a 90° cell and therefore $N \approx 4[\nu_y]$ cells. According to Eq. (3) and the property of the Bessel functions in Eq. (2), resonances should appear when $p = [\nu_y]$, $3[\nu_y]$, $5[\nu_y]$, $\cdots$, or when the wavelength $\lambda = 880$ m, 880/3 m, 880/5 m, $\cdots$. This effect is actually observed in Figure 5, although the SSC lattice that we used is much more complicated than the uniform FODO lattice.

4.2 Ground Waves from Point Sources

The closed-orbit separations due to waves produced by an oscillatory one-ton vertical force applied over a small area on the surface were calculated as a function of frequency for a variety of source locations. The medium was assumed to have elastic constants of $C_{11} = 18 \times 10^9$ newton/m^2 in compression, $C_{44} = 6 \times 10^9$ newton/m^2 in shear, a Poisson's ratio of $\sigma = 0.25$, and a density of

$\rho = 2000$ kg/m^3. The corresponding wave velocities are $v_p = 3.0$ km/sec for the compression body wave, $v_s = 1.73$ km/sec for the shear body wave, and $v_R = 1.59$ km/sec for the Rayleigh (surface) wave. At each quadrupole each of the three wave motions was analyzed for its components in the planes transverse to the local beam direction, so that closed-orbit effects could be calculated for each plane for all three waves. However, the Rayleigh wave dominated the closed-orbit effects; the results when the body waves were arbitrarily eliminated were hardly changed. Since ground motions has significant effects only for wavelength shorter than 880 m, we are concerned with frequency larger than 1.8 Hz only. No attenuation was assumed.

For a ground wave at a frequency lower than 1.8 Hz, the static solution ($\omega = 0$) can be used. For an exciting force of F_0, the vertical displacement u_z^s and radial displacement u_r^s computed by Fung[8] at a depth z and a radius r away are:

$$u_z^s = \frac{F_0}{4\pi C_{44} R}\left[2(1-\sigma) + \frac{z^2}{R^2}\right] ,$$

$$u_r^s = \frac{F_0}{4\pi C_{44} R}\left[\frac{rz}{R^2} - (1-2\sigma)\frac{r}{z+R}\right] , \qquad (7)$$

The calculated static vertical and radial amplitudes in the ground wave at 100-meter radius and 60-meter depth due to a one-ton force are about 0.002 micron and 0.0002 micron respectively. Note that these displacements are inversely proportional to the shear modulus or the square of the shear velocity.

Although we have determined that the ground wavelength is the most important propagation parameter for closed-orbit effects, here we must describe the source in terms of its frequency. In a vibrating-source problem there are generally three waves with three different wavelengths, and the only common parameter is the frequency of the source.

The ring geometry is shown in Figure 7. Figures 8a and 8b show the calculated vertical closed-orbit separations at the four beam crossings in the SSC due

to a 1-ton force vibrating on the surface at a point where the Southern Pacific Railroad crosses over the ring in the northwest section on the northern arc. This point is about 8 kilometers from the nearest low-beta interaction point (Low Beta 2).

In Figure 8a no attenuation due to absorption was assumed. As a result, all parts of the ring contribute substantially to the beam separation, since the dominant surface (Rayleigh) wave decreases only as $R^{-1/2}$. Also, a very complicated interference pattern is evident at each of the four beam interaction points.

If attenuation through absorption is included, exponentials of the form $e^{-\alpha r}$ and $e^{-\alpha z}$ are applied to the ground-wave distributions, where r and z represent the radial and vertical coordinates. The absorption coefficient is typically expressed in the form $\alpha = f/L_c$, L_c being the characteristic absorption length at 1 Hz.

In Figure 8b an absorption length of 10 km (at 1 Hz) is assumed. As a result the ground waves affect mainly the northwest sector of the northern arc, resulting in substantially smaller separations at the interaction points and a less complex beam-separation spectrum. A prominent feature of the separation spectrum in this case is a series of peaks, with spacings of about 14 Hz between the peaks. This structure is due to interference among the quadrupole magnets nearest the source of ground waves. In this geometry and with a FODO lattice having 90-degrees of phase shift per cell, the maxima are separated by v_R/L_h, where v_R is the velocity of the Rayleigh wave and L_h the half-cell length, which in this case was 111.25 m. Thus, $\Delta f = 1590/114.25 = 13.9$ Hz, as is evident in Figure 8b.

A case of particular interest is to have a source of ground waves directly above a low-beta interaction point, because of the sensitivity of the strong triplet quadrupole magnets to small disturbances. Figure 9 shows the separation spectra at the four interaction points due to a vibrating 1-ton force on the surface, 10 meters above the ring. In this case the separation spectra are characterized by maxima near 35 Hz and minima near 65 Hz. These characteristics are due to the

structure of the strong triplet quadrupole lenses, which dominate the separation spectrum both because of their high strengths and because of the high value of the beta functions in this region. Interference between the components of each triplet produce the maxima near 35 Hz and the minima near 65 Hz.

4.3 Ground Waves from Point Sources with Absorption

Comparison of FIgures 8a and 8b shows the significant effect of a characteristic absorption length of 10 km. More generally, since ground motion is important in all portions of the ring, not just near the interaction points, it was expected that characteristic absorption lengths equal to or smaller than the average diameter of the ring would be effective in reducing the ground motion effects, and that absorption lengths larger than the diameter would have little effect. Detailed computations have born out this expectation.

4.4 Ground Waves from Trains

Of particular concern at the SSC site are the effects of ground motion due to trains. In particular the Midlothian freight train crosses the collider ring in the northwest corner where the tunnel depth is at most only 10 m. Measurements at 100 feet from a Midlothian train are shown in Figure 4. However, it is not yet known what attenuation of such waves is to be expected.

If we consider the case of no attenuation, and assume a train made up of 100 cars, each exerting a vertically vibrating force of 100 tons, we have a model of 100 randomly correlated point sources whose closed-orbit effects add in quadrature. Thus, relative to the effects caused by the 1-ton force illustrated in Figure 8, such a train would be expected to produce effects that are $(\sqrt{100} \times 100 =)10^3$ greater. Calculations with trains of 100 cars extended over length of about 2 kilometers reduce this factor to 800. Thus, with no attenuation of the ground waves, this model produces closed-orbit differences at the low-beta crossings of up to 4.0 microns due to such a train at about 40 Hz. At Hera, an amplification factor of 10

attributed to the support of the quadrupole was observed. With such an amplification factor, this difference will become 40 microns. Such a differences would require a feedback correction ratio of about 80 in order to reduce the net difference to 1/10 of the beam r.m.s. radius. However, with an absorption attenuation length of $\alpha^{-1} = 10/f$ km, the closed-orbit difference with the same amplification will be 8 micron. Thus, unless the tunnel at the Midlothian crossing is deeper or the aborptive attenuation is larger, feedback correction will be necessary.

4.5 Effects of Wave Velocities

If we confine ourselves to the constant Q absorption model of Eq. (6), there is only one parameter to the elastic waves at a particular Poisson's ratio σ. We choose this parameter to be the compressional wave velocity v_p and fix σ at $\frac{1}{4}$. The displacement at depth z and radius r due to an harmonic point force F_0 of frequency f can be simplified to

$$a(r,z) \propto \left(\frac{F_0}{v_p^2}\right)\left(\frac{f}{v_p r}\right)^{\frac{1}{2}} e^{-\pi r f/Q v_p} e^{-4.66 z f/v_p} \ . \tag{8}$$

Here, only the surface wave has been included because it contributes mostly. The first exponential is absorption. The second exponential is the vertical attenuation of the surface wave according to Eq. (5). In fact, $b_2 = 4.66 f/v_p$ and $b_1 = 10.03 f/v_p$. Therefore, the b_1 term has been not been included.

Obviously, the maximum amplitude occurs at frequency

$$f = \frac{v_p}{2}\frac{1}{\pi r/Q + 4.66 z} \approx \frac{v_p}{2r} \ , \tag{9}$$

since the radius of response r is always much bigger than the depth z and the quality factor can be set approximately equal to π. Thus, the maximum amplitude is inversely proportional to v_p^2. Therefore, for a larger p-wave velocity, although the range of the damped spectrum extends to a higher frequency, the amplitude response itself will be very much smaller. As a result, the magnitude of v_p is extremely important in drawing any conclusion.

4.6 Effect of Size of Ring

Some may argue that many colliders have been in operation already; so we should not worry about the effects of ground motion to the SSC too. We think such a conclusion is incorrect. First, many colliders in operation are electron-positron or proton-antiproton colliders in which ground motion does not produce any separation at the two orbits. As for proton-proton colliders, the size of the SSC is much larger than any previous pp (or ee) collider, so that it is sensitive to a larger range of ground wavelengths. It was pointed out in Section 4.3 that ground motion will affect the closed-orbit deviation only up to a frequency of 4.5 Hz, because of the greater attenuation at higher frequencies. Even if we assume a surface wave velocity of $v_R = 531$ m/s (or $v_p = 1$ km/s), we need not worry about wavelengths that are shorter than $531/4.5 = 118$ m for any pp or ee collider, because of the greater attenuation at these shorter wavelengths. The corresponding minimum wavelength of concern at $v_R = 1.59$ km/s (or $v_p = 3$ km/s) is 354 m. For a small collider, the betatron wavelength is usually less than this figure. In the ISR, for example, the betatron wavelength was 106 m. For the SSC, however, the betatron wavelength is about 880 m. Therefore, ground-motion effects may be significant.

5. CONCLUSIONS

We see that ground motion effects at the site due to trains, and possibly highway traffic also, could produce significant reduction in luminosity if not compensated somehow. Measurements of ground motion amplitude at many representative points of the tunnel and also of the absorption coefficients are required before dependable conclusions can be reached. The SSC site in Texas is much more complicated than the simple model employed here, so that our results are only suggestive of the magnitude of the effects to be expected.

APPENDIX

A.1 Elastic Moduli

Hooke's Law states that there is a linear relationship between stress τ_{ij} and strain S_{ij}. Since τ_{ij} and S_{ij} are symmetric tensors of rank two under rotation, the most general Hooke's Law for an isotropic medium can be written as

$$\tau_{ij} = \lambda(\mathrm{Tr}\, S)\delta_{ij} + 2\mu S_{ij} \quad , \tag{A.1}$$

where λ and μ are called Lamé moduli and are scalars under rotation. There are many other moduli for a medium. But they can all be expressed in terms of λ and μ.

Consider the body in Figure 9 under the shear stress $\tau_{xy} = \tau_{yx} = T$ while all the other components of τ_{ij} are zero. The body $ABCD$ is distorted into $AB'C'D'$. From Eq. (A.1), it is clear that the strain

$$S_{xy} = S_{yx} = \frac{T}{2\mu} \tag{A.2}$$

while all the other components are zero. We therefore conclude that μ is in fact the shear modulus. The shearing angle is

$$\gamma = 2S_{xy} \tag{A.3}$$

and has been customarily called the "shear strain."

In the situation of a simple tension

$$\tau_{ij} = \begin{pmatrix} T & 0 & 0 \\ 0 & 0 & 0 \\ 0 & 0 & 0 \end{pmatrix} \tag{A.4}$$

we obtain from Eq. (A.1), the strain

$$S_{ij} = \frac{T}{2\mu} \begin{pmatrix} \frac{2(\lambda+\mu)}{3\lambda+2\mu} & 0 & 0 \\ 0 & -\frac{\lambda}{3\lambda+2\mu} & 0 \\ 0 & 0 & -\frac{\lambda}{3\lambda+2\mu} \end{pmatrix} \quad . \tag{A.5}$$

Therefore the ordinary Young modulus for tension is

$$Y = \frac{\text{longitudinal stress}}{\text{longitudinal strain}} = \frac{\mu(3\lambda + 2\mu)}{\lambda + \mu} \quad , \tag{A.6}$$

and the Poisson's ratio

$$\sigma = \frac{\text{lateral shrink}}{\text{longitudinal stretch}} = \frac{\lambda}{2(\lambda + \mu)} \tag{A.7}$$

When an isotropic pressure p is applied, $\tau_{ij} = -p\delta_{ij}$. The strain $S_{ij} = S\delta_{ij}$ is also isotropic. The fractional increase in length obtained from Eq. (A.1) is

$$S = -\frac{p}{3\lambda + 2\mu} \quad . \tag{A.8}$$

Dilation θ is defined as the trace of S_{ij} on the sum of fractional stretches in the three directions. The bulk modulus is therefore

$$k = -\frac{p}{\theta} = \lambda + \frac{2\mu}{3} \quad . \tag{A.9}$$

For a fluid that can flow freely, the shear modulus vanishes, and λ is then just the bulk modulus.

The component S_{ij} of the strain tensor is defined as the change in displacement or distortion u_i in the i-direction relative to a point unit distance away in the j-direction. We assume that the body will not be displaced or rotated as a whole under the action of the applied stress. Therefore

$$S_{ij} = \frac{1}{2}\left(\partial_i u_j + \partial_j u_i\right) \quad . \tag{A.10}$$

A.2 Equation of Motion

Consider the cubic element $dxdydz$ in Figure 11 subjected to a stress τ_{ij}. For the x-direction, the displacement u_x is given by

$$\left[\rho\frac{\partial^2 u_x}{\partial t^2}\right] dxdydz = \left[\frac{\partial \tau_{xx}}{\partial x}\, dx\right] dydz + \left[\frac{\partial \tau_{yx}}{\partial y}\, dy\right] dzdx + \left[\frac{\partial \tau_{zx}}{\partial z}\, dz\right] dxdy \ , \quad \text{(A.11)}$$

where ρ is the density of the body. The right side represents the force acting on the cubic element due to stresses on each of its six surfaces. For example, the first square bracket on the right side is the difference in compressional stresses on the two surfaces normal to the x-axis, the second square bracket is the difference in shear stresses on the two surfaces normal to the y-axis, etc. In tensor notation, Eq. (A.11) generalizes to

$$\rho\frac{\partial^2 u_i}{\partial t^2} = \partial_j \tau_{ji} \ . \quad \text{(A.12)}$$

Applying Hooke's Law [Eq. (A.1)] and the explicit relation between strain and displacement [Eq. (A.10)], Eq. (A.12) can be written in vector form as

$$\rho\frac{\partial^2 \vec{u}}{\partial t^2} = (\lambda + 2\mu)\,\vec{\nabla}(\vec{\nabla}\cdot\vec{u}) - \mu\vec{\nabla}\times\vec{\nabla}\times\vec{u} \ . \quad \text{(A.13)}$$

The displacement vector can be written as

$$\vec{u} = \vec{u}_p + \vec{u}_s \ , \quad \text{(A.14)}$$

where $\vec{u}_p$ is irrotational and $\vec{u}_s$ divergenceless, or

$$\vec{\nabla}\times\vec{u}_p = 0 \quad \text{and} \quad \vec{\nabla}\cdot\vec{u}_s = 0 \ . \quad \text{(A.15)}$$

Obviously $\vec{u}_p$ implies dilational motion and $\vec{u}_s$ shear motion. The equation of

motion (A.13) will therefore be satisfied by two wave equations:

$$\rho \frac{\partial^2 \vec{u}_p}{\partial t^2} = (\lambda + 2\mu)\ \nabla^2 \vec{u}_p \quad , \tag{A.16}$$

and

$$\rho \frac{\partial^2 \vec{u}_s}{\partial t^2} = \mu \nabla^2 \vec{u}_s \quad . \tag{A.17}$$

The former describes a longitudinal or compressional wave with velocity

$$v_p = \sqrt{\frac{\lambda + 2\mu}{\rho}} \quad , \tag{A.18}$$

while the latter describes a shear wave with velocity

$$v_s = \sqrt{\frac{\mu}{\rho}} \quad . \tag{A.19}$$

In Section 2.3 above, we have used the notations $C_{11} = \lambda + 2\mu$ and $C_{44} = \mu$. Obviously, we must have $v_p > v_s$. The ratio of the two wave velocities can be expressed as a function of the Poisson's ratio only. In fact using Eq. (A.7),

$$\frac{v_p}{v_s} = \sqrt{\frac{2(1-\sigma)}{1-2\sigma}} \tag{A.20}$$

which gives $\sqrt{3}$ for $\sigma = \frac{1}{4}$ and decreases to $\sqrt{2}$ for $\sigma = 0$. For a free-flowing fluid ($\sigma = \frac{1}{2}$), the shear modulus $\mu = 0$. Thus, $v_s = 0$ or the shear wave cannot propagate.

Unlike the electromagnetic waves, here we have a longitudinal component that travels with a different velocity. Bouncing off from a boundary, a pure compressional wave or a pure shear wave can have a compressional reflected component plus a shear component at different reflection angles determined by Snell's Law. Similar consideration applies for waves transmitted across a boundary.

A.3 Surface Wave

When the medium is an infinite half space ($z = 0$ to ∞), the equation of motion (A.13) admits a solution with z-dependency e^{-bz} where b is real and positive. This is very similar to (but not the same as) the wave created at the surface of a pond by dropping in a piece of rock. The amplitude will decay exponentially inside the water. This wave is called the surface wave or Rayleigh wave, which travels with a particular velocity v_R as demonstrated below.

Consider a two-dimensional example ($u_y = 0$) with displacements

$$\begin{cases} u_x = Ae^{-bz}e^{i(k_R x - v_R t)} \\ u_z = Be^{-bz}e^{i(k_R x - v_R t)} \end{cases} , \tag{A.21}$$

where A and B are constant and k_R the wave number. Substituting into the wave equation (A.13) which can be rewritten in terms of v_p and v_s as

$$\frac{\partial^2 \vec{u}}{\partial t^2} = \left(v_p^2 - v_s^2\right) \vec{\nabla}\left(\vec{\nabla} \cdot \vec{u}\right) - v_s^2 \nabla^2 \vec{u} , \tag{A.22}$$

we obtain a nontrivial solution ($A \neq 0$, $B \neq 0$)

$$\left[v_p^2 b^2 - \left(v_p^2 - v_R^2\right) k_R^2\right] \left[v_s^2 b^2 - \left(v_s^2 b^2 - c_R^2\right) k_R^2\right] = 0 . \tag{A.23}$$

The two possible roots for b are

$$b_1 = k_R \sqrt{1 - \frac{v_R^2}{v_p^2}} \quad \text{and} \quad b_2 = k_R \sqrt{1 - \frac{v_R^2}{v_s^2}} . \tag{A.24}$$

In order that b is real, the Rayleigh velocity v_R must therefore be less than v_s and v_p, or

$$v_R < v_s < v_p . \tag{A.25}$$

For each root A and B will be related. The general solution can then be written

as

$$\begin{pmatrix} u_x \\ \\ u_z \end{pmatrix} = \begin{pmatrix} 1 & 1 \\ \\ ib_1/k_R & ik_R/b_2 \end{pmatrix} \begin{pmatrix} A_1 e^{-b_1 z} \\ \\ A_2 e^{-b_2 z} \end{pmatrix} \quad , \tag{A.26}$$

where the common exponential factor $\exp\left[k_R(x - v_R t)\right]$ has been omitted.

Finally we enforce the boundary condition at the free surface $z = 0$:

$$\tau_{zx} = \tau_{zy} = \tau_{zz} = 0 \quad . \tag{A.27}$$

In view of Eq. (A.10) and Hooke's Law, they are equivalent to

$$\frac{\partial u_x}{\partial z} + \frac{\partial u_z}{\partial x} = 0 \quad , \tag{A.28}$$

$$\left(v_p^2 - 2v_s^2\right)\left(\frac{\partial u_x}{\partial x} + \frac{\partial u_z}{\partial z}\right) - 2v_s^2 \frac{\partial u_z}{\partial z} = 0 \quad , \tag{A.29}$$

where Eqs. (A.18) and (A.19) have been used. To satisfy these two equations nontrivially at $z = 0$ (i.e., $A_1 \neq 0$, $A_2 \neq 0$), we must have

$$F_R\left(\frac{v_p}{v_R}\right) = 0 \tag{A.30}$$

where the Rayleigh function $F_R(\zeta)$ is defined as

$$F_R(\zeta) = \left(2\zeta^2 - \eta^2\right)^2 - 4\zeta^2 \left(\zeta^2 - \eta^2\right)^{\frac{1}{2}} \left(\zeta^2 - 1\right)^{\frac{1}{2}} \quad , \tag{A.31}$$

with

$$\eta = \frac{v_p}{v_s} \quad . \tag{A.32}$$

Equation (A.30) is a cubic in ζ^2 or $(v_p/v_R)^2$. However, only one root will satisfy condition (A.25). Therefore, there can be only one Rayleigh velocity in a medium. Again the ratio v_R/v_s or v_R/v_p depends on the Poisson's ratio only. The ratio v_R/v_s varies almost linearly from 0.874 to 0.942 when the Poisson's ratio σ changes from 0 to 0.4. For the more common $\sigma = 0.25$, $v_R/v_s = 0.9194$.

From Eq. (A.26), we see that the vertical displacement leads the horizontal displacement by $\pi/2$, implying that the particle motion for Rayleigh waves is elliptical retrograde, or rotating backward to the direction of wave propagation. The Rayleigh wave number k_R, which equals ω/v_R at frequency $\omega/2\pi$, is related to the compressional wave number k_p by

$$k_R = \frac{v_p}{v_R} k_p \ . \tag{A.33}$$

A wave created at the surface of a pond by dropping a piece of pebble is in fact very different from the Rayleigh surface wave we discussed above, both physically and mathematically. In the above derivation, it is clear that the existence of Rayleigh wave depends on the presence of *both* the longitudinal and transverse waves. For a perfect fluid, however, there is no transverse wave because the shear modulus vanishes. Here, it is gravity that provides the transverse oscillations and leads to the creation of surface waves in fluids. In fact, the fluid particles in the surface wave are *not* elliptically retrogade but rotate instead forward to the direction of the wave motion.

A.4 Waves Due to an Harmonic Point Source

Here we use cylindrical coordinates (r, ϕ, z). The equation of motion (A.13) or (A.22) is solved subject to the boundary conditions at the earth's surface $(z = 0)$

$$\tau_{zz} = \begin{cases} P_0 e^{-i\omega t} & r < a \\ 0 & r \geq a \end{cases}$$

$$\tau_{zr} = \tau_{z\phi} = 0 \tag{A.34}$$

where $F_0 = \pi a^2 P_0$ is the amplitude of the harmonic force at frequency $\omega/2\pi$. The radius a of the source will go to zero eventually. This problem was first solved by Miller and Pursey, and we are giving here only a brief description of the solution.

This problem is ϕ-independent. Hankel transform is used to transform the coordinate r to ζ. So, to obtain the displacements at a point, we need only to solve differential equations in z and perform universe Hankel transforms. However, the inverse Hankel transforms are non-trivial because of branch points due to the occurrence of terms like $\sqrt{\zeta^2-k_p^2}$ and $\sqrt{\zeta^2-k_s^2}$, where k_p and k_s are respectively the compressional wave number and shear wave number. Only the far fields can be evaluated in closed forms using the method of steepest descent. The final result gives for body wave

$$u_R \sim -\frac{P_0 a^2}{2C_{44}} \frac{e^{ik_p R}}{k_p R} \frac{\left(\eta^2 - 2\sin^2\theta\right)\cos\theta}{F_R\left(\sin\theta\right)} , \tag{A.35}$$

$$u_\theta \sim -\frac{iP_0 a^2 \eta^3}{2C_{44}} \frac{e^{-i\eta k_s R}}{k_p R} \frac{\sqrt{\eta^2\sin^2\theta - 1}\sin 2\theta}{F_R(\eta\sin\theta)} , \tag{A.36}$$

and for the surface wave

$$u_z \sim \frac{P_0 a^2 e^{-i\pi/4}}{C_{44} F_R'(p)} \sqrt{\frac{\pi k_p p(p^2-1)}{2r}} \left\{ 2p^2 e^{-b_2 z} - \left(2p^2-\eta^2\right) e^{-b_1 z} \right\} e^{ik_p r} , \tag{A.37}$$

$$u_r \sim \frac{P_0 a^2 e^{i\pi/4}}{C_{44} F_R'(p)} \sqrt{\frac{\pi k_p p^3}{2r}} \left\{ 2\sqrt{p^2-1}\sqrt{p^2-\eta^2} e^{-b_2 z} - \left(2p^2-\eta^2\right) e^{-b_1 z} \right\} e^{ik_p p r} . \tag{A.38}$$

Again the time dependent factor has been omitted. The various displacement u_R, u_θ, u_z, u_r, and the conical angle θ are defined in Figure 12. In above $F_R(\zeta)$ is the Rayleigh function defined in Eq. (A.31) and p is its legitimate pole. The exponents $b_1 z$ and $b_2 z$ designating the decay of the surface wave with depth are defined in Eq. (A.24).

The power going into each wave can be computed by integrating the fields at an hemisphere of large radius R. The power into the surface wave is

$$W_{\rm sur} = \frac{\pi\omega^2 a^4 P_0^2 \eta^2}{\rho v_p^3} \int_0^\infty X(k_p z)\, d(k_p z) \ , \tag{A.39}$$

where

$$\begin{aligned} X(k_p z) = \frac{\pi(2p^2-\eta^2)}{4\left[F_R'(p)\right]^2} \Big\{ & 4p^2(p^2-1)\left[2p^2 e^{-b_2 z} - (2p^2-\eta^2)e^{-b_1 z}\right] \\ & \times \left(e^{-b_2 z} - e^{-b_1 z}\right) + \left(2p^2-\eta^2\right)\left[\left(2p^2-\eta^2\right)e^{-b_2 z} - 2p^2 e^{-b_1 z}\right] \\ & \times \left[\left(2p^2-\eta^2\right)e^{-b_2 z} - \left(2p^2+\eta^2-2\right)e^{-b_1 z}\right] \Big\} \ , \end{aligned} \tag{A.40}$$

and can be integrated in closed form. The powers into the compressional wave and the shear wave are

$$W_p = \frac{\pi\omega^2 a^4 P_0^2 \eta^4}{4\rho v_p^3} \int_0^{\frac{\pi}{2}} \left[\frac{\left(\eta^2 - 2\sin^2\theta\right)\cos\theta}{F_R(\eta\sin\theta)}\right]^2 \sin\theta\, d\theta \ , \tag{A.41}$$

$$W_s = \frac{\pi\omega^2 a^4 P_0^2 \eta^4}{4\rho v_p^3} \int_0^{\frac{\pi}{2}} \left|\frac{\sin 2\theta\sqrt{\eta^2\sin^2\theta - 1}}{F_R(\eta\sin\theta)}\right|^2 \sin\theta\, d\theta \ . \tag{A.42}$$

When Poisson's ratio is $\sigma = 0.25$, we get

$$W_{\rm sur} : W_p : W_s = 3.257 : 0.333 : 1.246 \tag{A.43}$$

or 67.3% of the power goes into the surface wave. The partition of power for other values of the Poisson's ratio is given in Table 1. The numbers are in units of $\pi\omega^2 a^4 P_0^2/4\rho v_p^3$ and the numbers enclosed in parentheses are the fractional shares.

Table 1. Partitions of power between elastic waves.

Poisson's Ratio	Compressional Wave		Shear Wave		Surface Wave		Sum
0.0000	0.2081	(.055)	0.7027	(.185)	2.8917	(.760)	3.8025
0.0500	0.2260	(.059)	0.7561	(.197)	2.8620	(.745)	3.8441
0.1000	0.2486	(.063)	0.8142	(.207)	2.8644	(.729)	3.9272
0.1500	0.2753	(.067)	0.9142	(.223)	2.9123	(.710)	4.1019
0.2000	0.3044	(.070)	1.0390	(.238)	3.0291	(.693)	4.3725
0.2500	0.3330	(.069)	1.2467	(.258)	3.2578	(.673)	4.8375
0.3000	0.3574	(.063)	1.5985	(.283)	3.6902	(.654)	5.6462
0.3500	0.3736	(.052)	2.3060	(.319)	4.5577	(.630)	7.2373
0.4000	0.3776	(.035)	3.9046	(.357)	6.6399	(.608)	10.9221
0.4500	0.3658	(.014)	10.2619	(.405)	14.6977	(.580)	25.3254

REFERENCES

1. It is interesting to note that this effect does not occur in a single-ring p-$\bar{p}$ collider because in such a ring the two beams have a common magnetic closed orbit.

2. J. Rossbach, "Closed-Orbit Distortions of Periodic FODO Lattices due to Plane Ground Waves," Particle Accelerators, 1988, Vol. 23, p. 121.

3. J. T. Nelson, "SSC Environmental Ground Vibration Study," SSC-N-307, January 1987.

4. G. F. Miller and H. Pursey, "On the Partition of Energy between Elastic Waves in a Semi-Infinite Solid," Proc. Royal Soc., A233, 1955, p. 55.

5. G. E. Fischer and P. Morton, "Ground Motion Tolerances for the SSC," SSC-55, January 1986.

6. K. Aki and P. Richards, "Quantitative Seismology," 1980, Vol. 1, Chapter 10.

7. A. A. Garren and D. E. Johnson, "The 90° SSC Lattice," September 1987.

8. Y. C. Fung, "Foundation of Solid Mechanics," Prentice Hall, New Jersey, 1965.

List of Figure Captions

Fig. 1. Closed-orbit perturbation due to a transverse shift of a quadrupole in the y-direction at $s = 0$, as described by Eq. (1).

Fig. 2. Vertical response of the European Synchrotron Radiation Facility (ESRF) to plane ground waves. Ring circumference is $C = 850$ m, vertical tune $\nu_y = 19.2$ and number of cells $N = 80$. Upper plot shows response (r.m.s. response in dashes) as a function of C/λ for wave direction $\theta_w = 0$. The response increases as C/λ passes through η_y, $N - [\nu_y]$, $N + [\nu_y]$, ... The lower plot shows response as a function of θ_w with C/λ fixed at $N \quad [\nu_y]$.

Fig. 3. Power spectra of microseismic noise at noisy and quiet conditions for a typical station on hard basement rock.

Fig. 4a. Ground motion at 100 feet from a railroad near the SSC site as a function of time.

Fig. 4b. The railroad vibration spectrum 100 feet from the track.

Fig. 4c. The ground vibration signal from a quarry blast about 6 miles from the quarry.

Fig. 4d. The vibration spectrum from a quarry shot.

Fig. 5a. Vertical beam separation at a low-beta crossing caused by plane waves in the east/west direction (for the SSC ring long axis in the north/south direction). The ground waves have a 1-micron vertical displacement at each wavelength.

Fig. 5b. Vertical beam separation at a medium-beta crossing caused by plane waves in the east/west direction. The ground wave vertical amplitude is 1 micron at each wavelength.

Fig. 5c. Vertical beam separation at a low-beta crossing caused by plane waves in the NE/SW direction. The ground wave vertical amplitude is 1 micron at each wavelength.

Fig. 5d. The vertical beam separation at a medium-beta crossing caused by a plane wave in the NE/SW direction. The ground wave vertical amplitude is 1 micron at each wavelength.

Fig. 6a. Vertical beam separation at a low-beta crossing caused by plane waves of 880-meter wavelength at various angles of incidence. The short axis of the SSC corresponds in this plot to about 9 degrees. The vertical amplitude of the ground wave is 1 micron.

Fig. 6b. Vertical beam separation at a low-beta crossing caused by plane waves of 500-meter wavelength at various angles of incidence. The SSC short-axis is at about 9 degrees in this plot. The vertical amplitude of the ground wave is 1 micron.

Fig. 6c. Vertical beam separation at a medium-beta crossing caused by a plane wave of 880-meter wavelength at various angles of incidence. The vertical amplitude of the groundwave is 1 micron.

Fig. 6d. Vertical beam separation at a medium-beta crossing caused by a plane wave of 500-meter wavelength at various angles of incidence. The amplitude of the ground wave is 1 micron.

Fig. 7. Layout of the SSC ring.

Fig. 8a. The spectrum of the vertical beam separation at the four interaction points due to ground waves from a vibrating source located on the surface in the northwest region of the northern arc where the South Pacific Railroad crosses over the SSC ring. The source is a 1-ton vertical force at each frequency. The tunnel depth is taken as 10 meters and uniform. No attenuation due to absorption was assumed.

Fig. 8b. The spectrum of the vertical beam separation at the four interaction points, as in Figure 8a, but with a characteristic absorption length of 10 km (at 1 Hz).

Fig. 9. The spectrum of the vertical beam separation at the four interaction points when the 1-ton vibrating force is directly over the Low-Beta-1 interaction point.

Fig. 10. A body distorted by pure shear stress T.

Fig. 11. The force in the x-direction due to stresses on the six surfaces of a cubic element.

Fig. 12. Vertical point load on surface of elastic half-space.

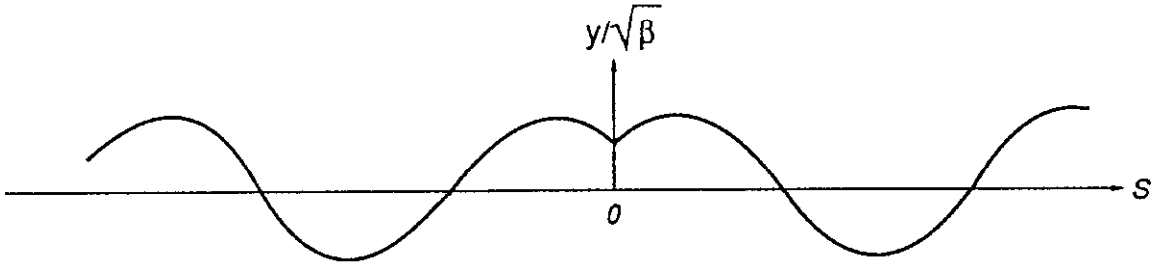

Fig. 1. Closed-orbit perturbation due to a transverse shift of a quadrupole in the y-direction at $s = 0$, as described by Eq. (1).

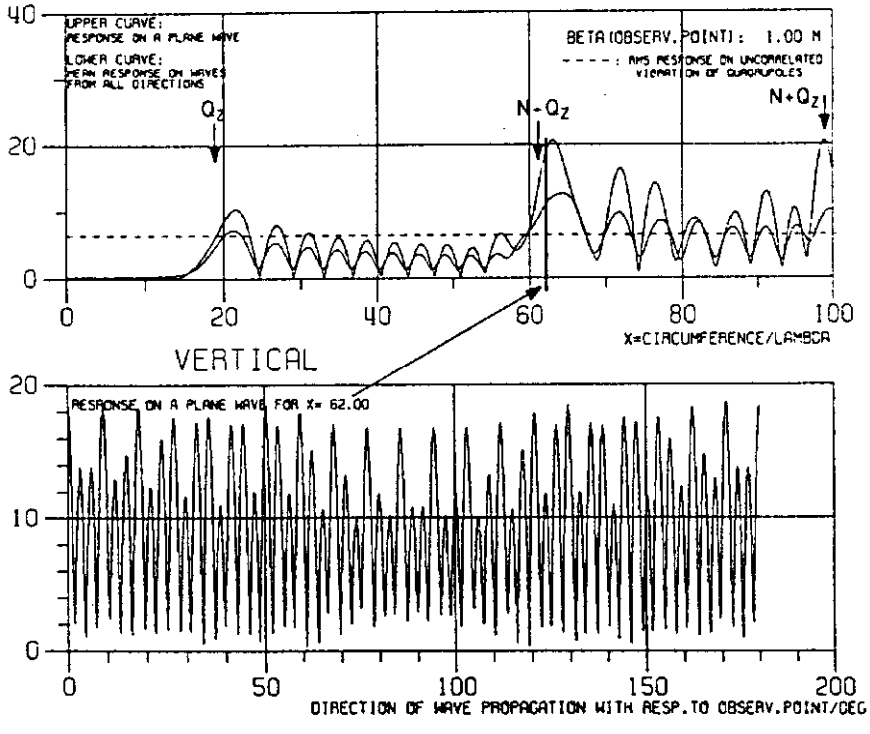

Fig. 2. Vertical response of the European Synchrotron Radiation Facility (ESRF) to plane ground waves. Ring circumference is $C = 850$ m, vertical tune $\nu_y = 19.2$ and number of cells $N = 80$. Upper plot shows response (r.m.s. response in dashes) as a function of C/λ for wave direction $\theta_w = 0$. The response increases as C/λ passes through η_y, $N - [\nu_y]$, $N + [\nu_y]$, ... The lower plot shows response as a function of θ_w with C/λ fixed at $N - [\nu_y]$.

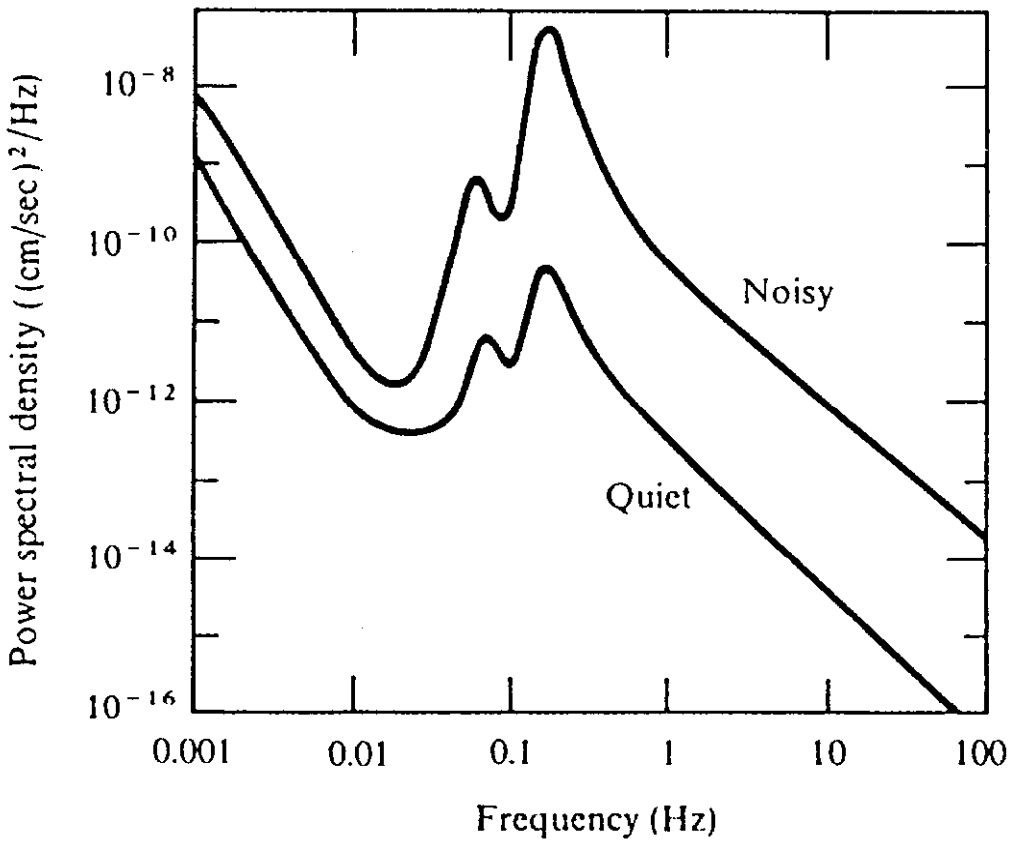

Fig. 3. Power spectra of microseismic noise at noisy and quiet conditions for a typical station on hard basement rock.

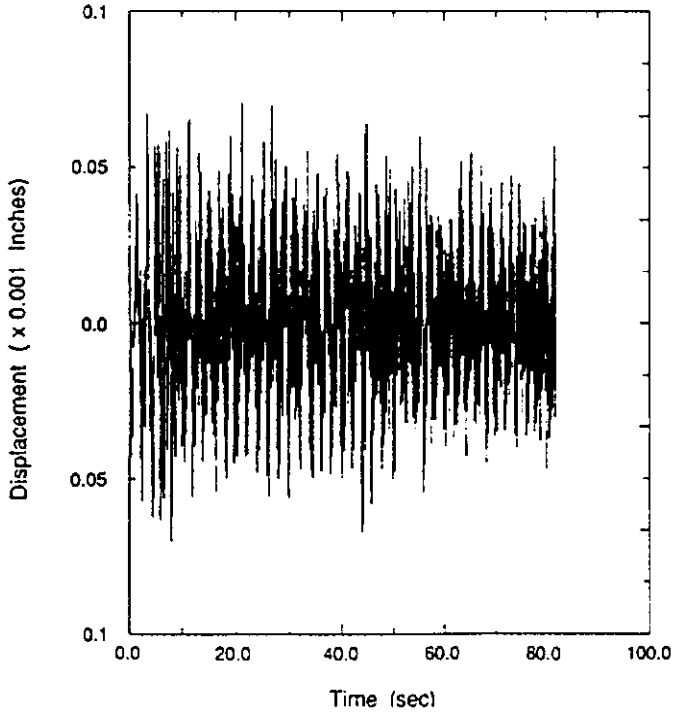

Fig. 4a. Ground motion at 100 feet from a railroad near the SSC site as a function of time.

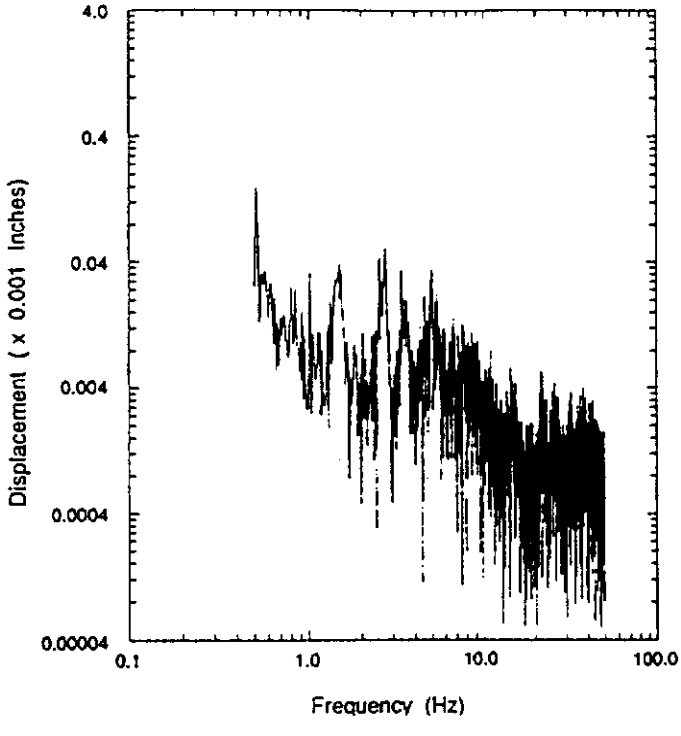

Fig. 4b. The railroad vibration spectrum 100 feet from the track.

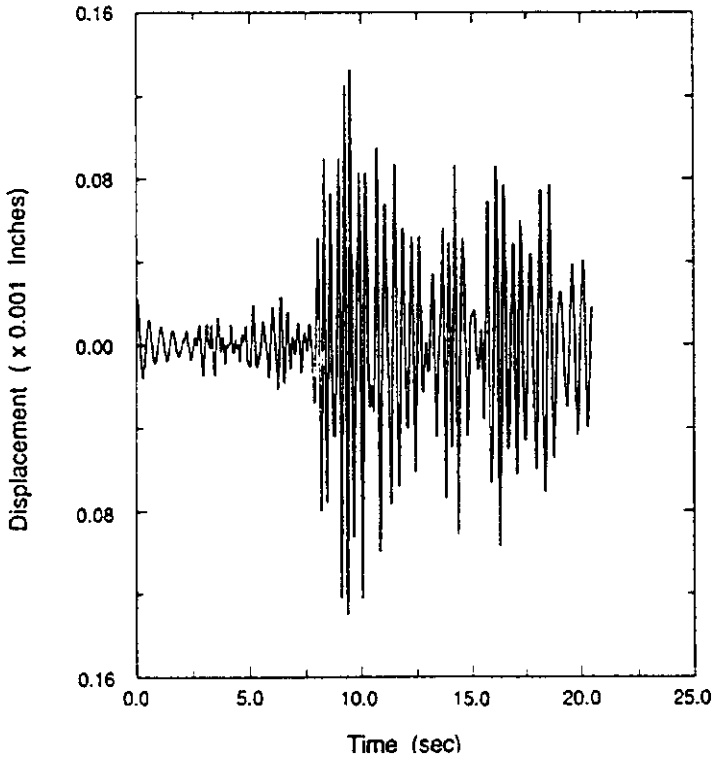

Fig. 4c. The ground vibration signal from a quarry blast about 6 miles from the quarry.

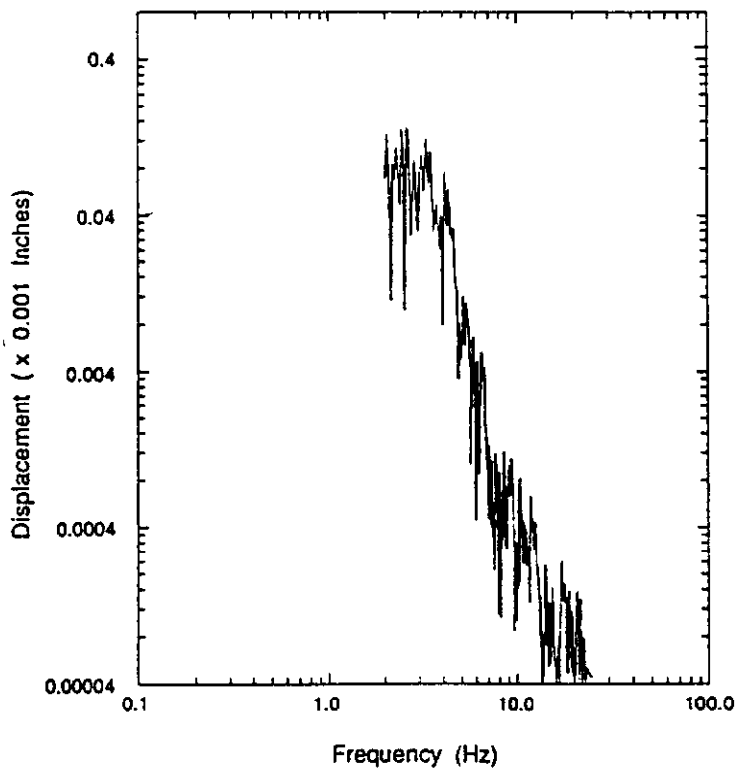

Fig. 4d. The vibration spectrum from a quarry shot.

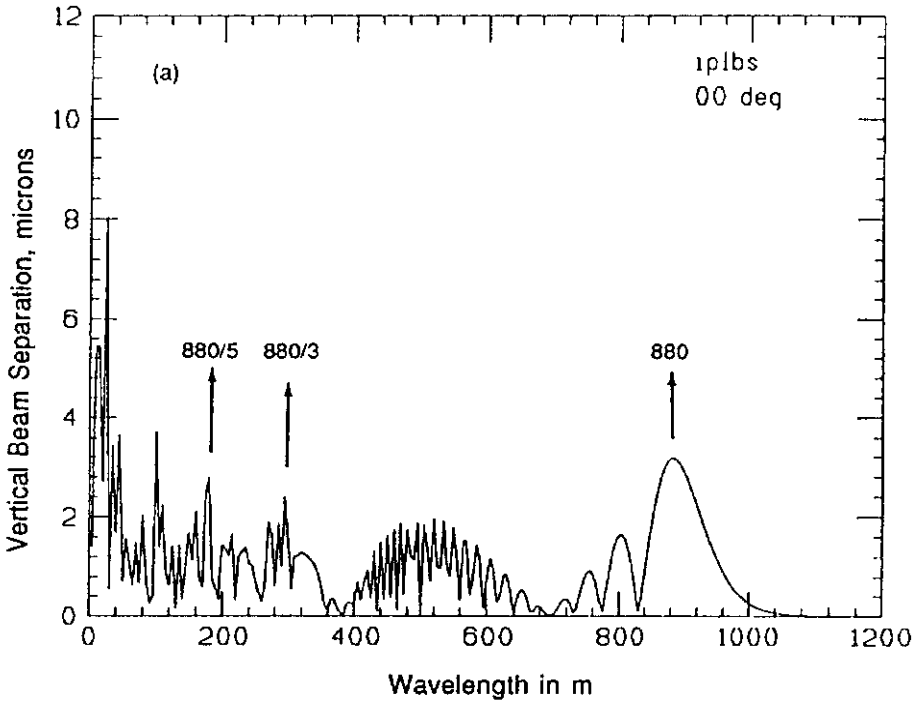

Fig. 5a. Vertical beam separation at a low-beta crossing caused by plane waves in the east/west direction (for the SSC ring long axis in the north/south direction). The ground waves have a 1-micron vertical displacement at each wavelength.

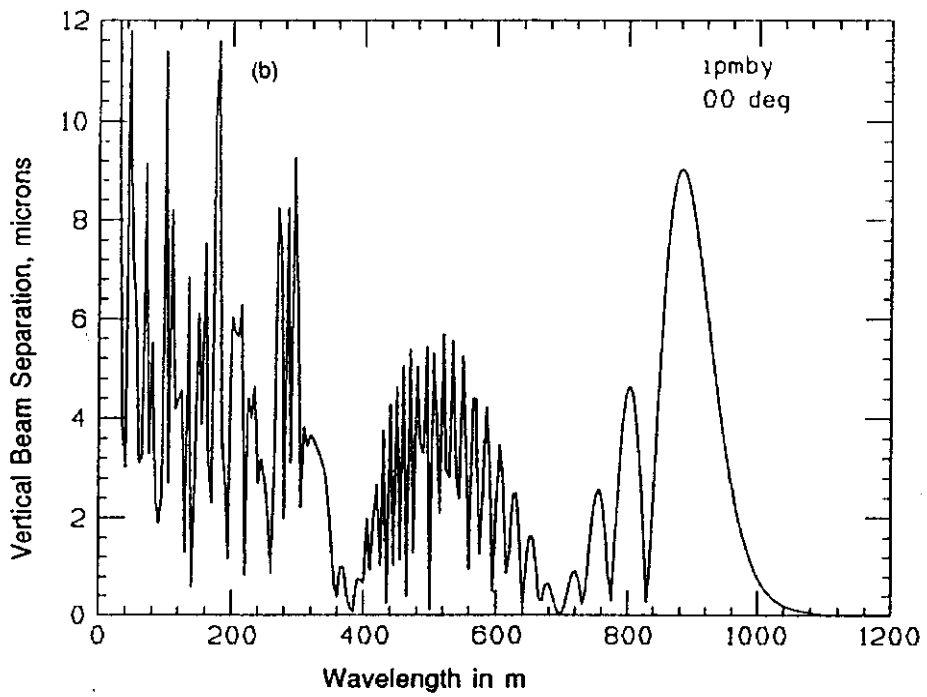

Fig. 5b. Vertical beam separation at a medium-beta crossing caused by plane waves in the east/west direction. The ground wave vertical amplitude is 1 micron at each wavelength.

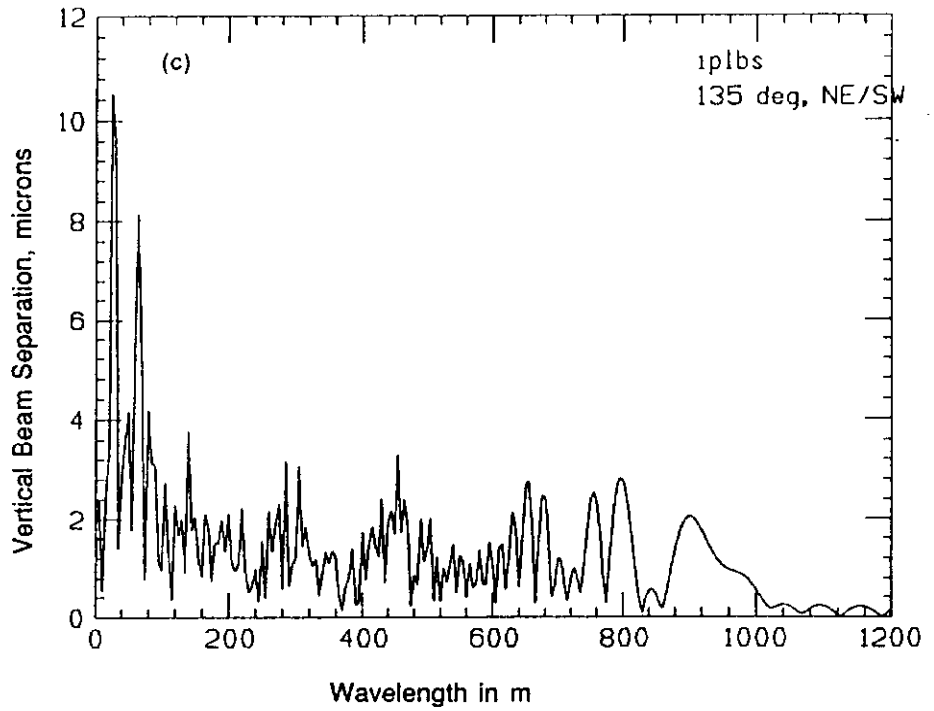

Fig. 5c. Vertical beam separation at a low-beta crossing caused by plane waves in the NE/SW direction. The ground wave vertical amplitude is 1 micron at each wavelength.

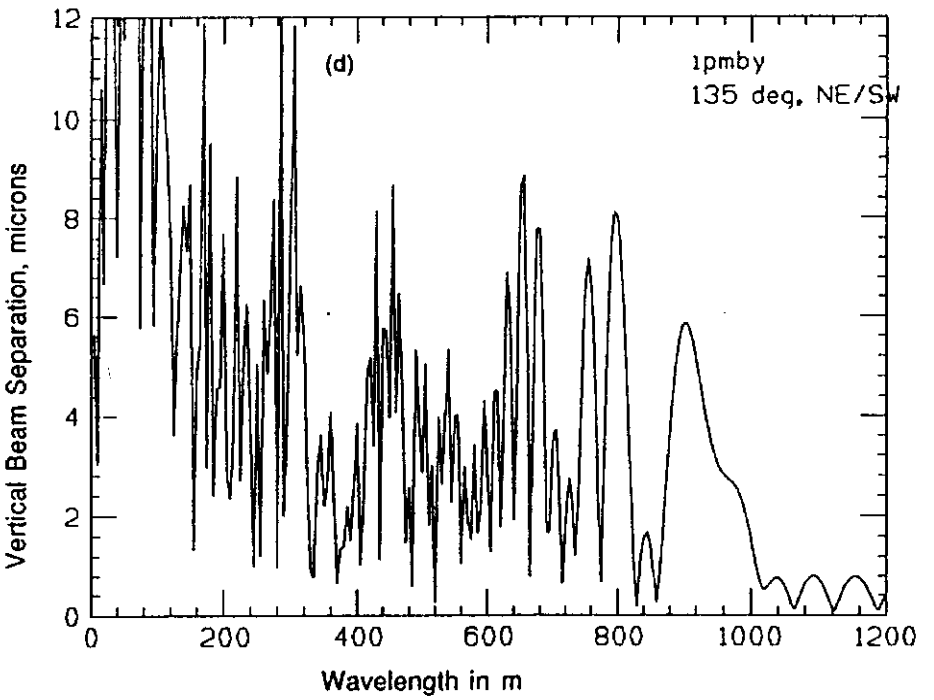

Fig. 5d. The vertical beam separation at a medium-beta crossing caused by a plane wave in the NE/SW direction. The ground wave vertical amplitude is 1 micron at each wavelength.

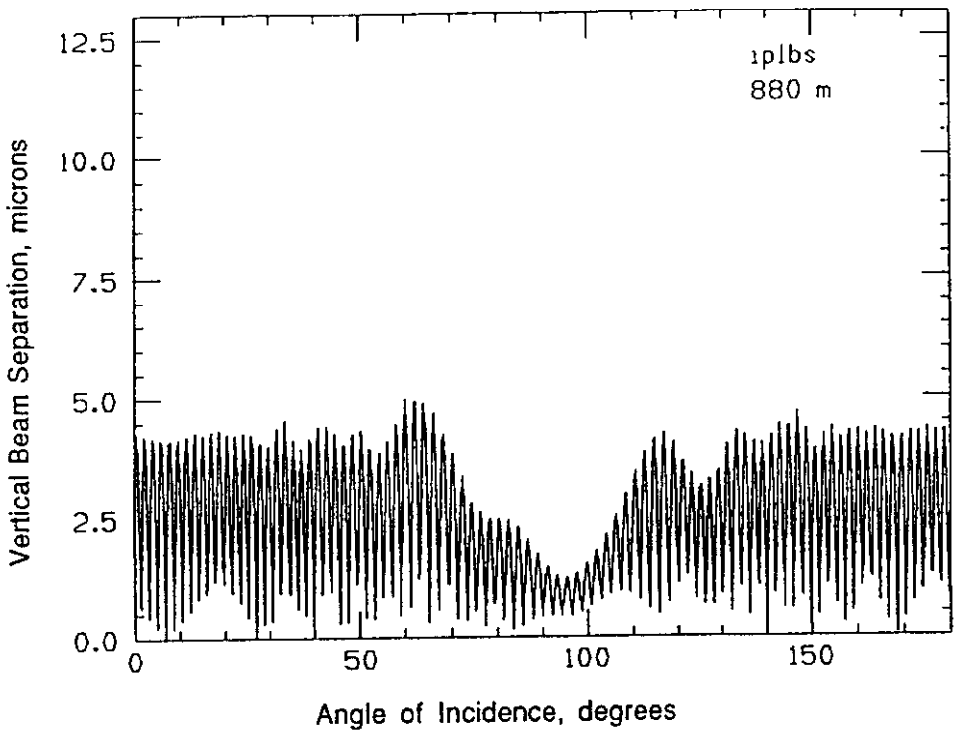

Fig. 6a. Vertical beam separation at a low-beta crossing caused by plane waves of 880-meter wavelength at various angles of incidence. The short axis of the SSC corresponds in this plot to about 9 degrees. The vertical amplitude of the ground wave is 1 micron.

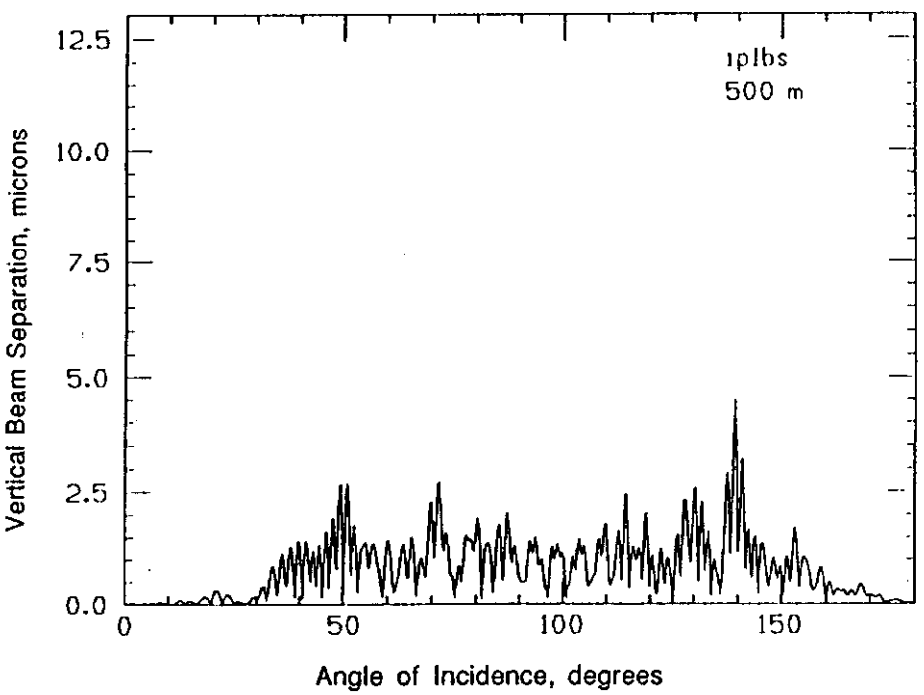

Fig. 6b. Vertical beam separation at a low-beta crossing caused by plane waves of 500-meter wavelength at various angles of incidence. The SSC short-axis is at about 9 degrees in this plot. The vertical amplitude of the ground wave is 1 micron.

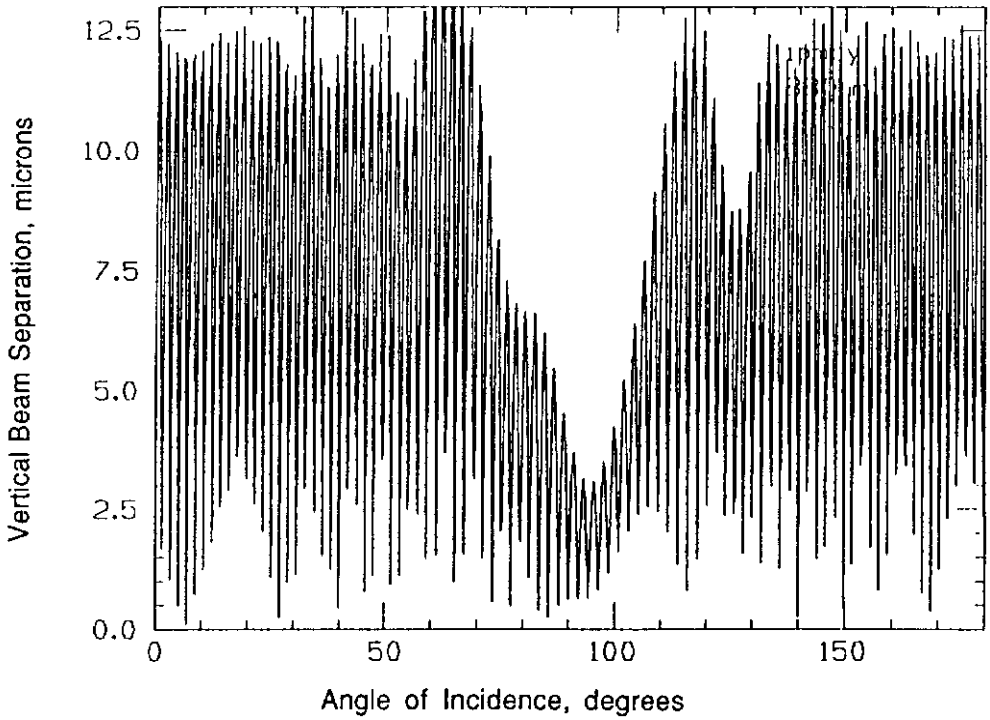

Fig. 6c. Vertical beam separation at a medium-beta crossing caused by a plane wave of 880-meter wavelength at various angles of incidence. The vertical amplitude of the groundwave is 1 micron.

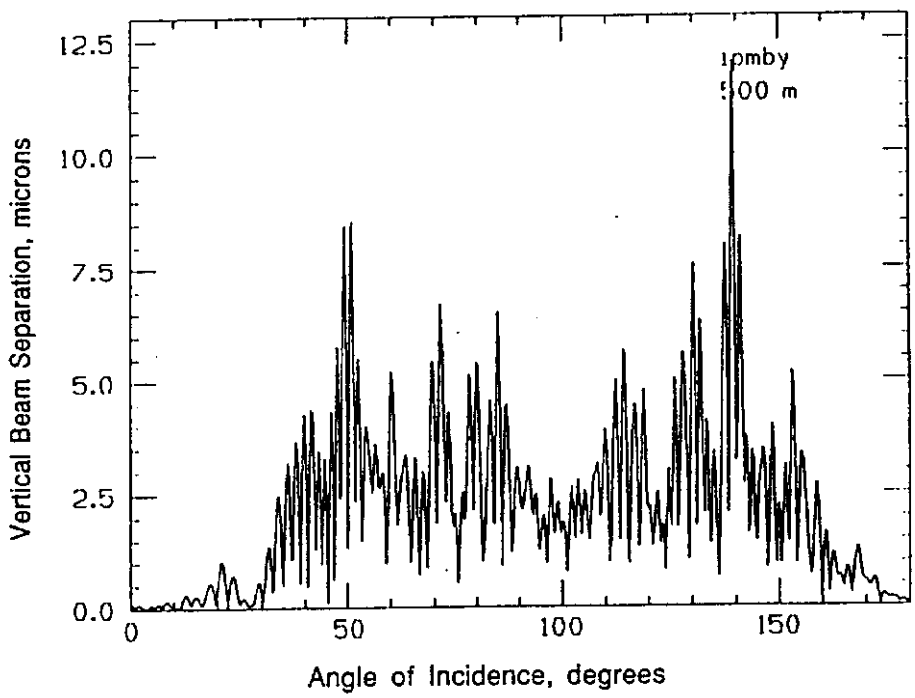

Fig. 6d. Vertical beam separation at a medium-beta crossing caused by a plane wave of 500-meter wavelength at various angles of incidence. The amplitude of the ground wave is 1 micron.

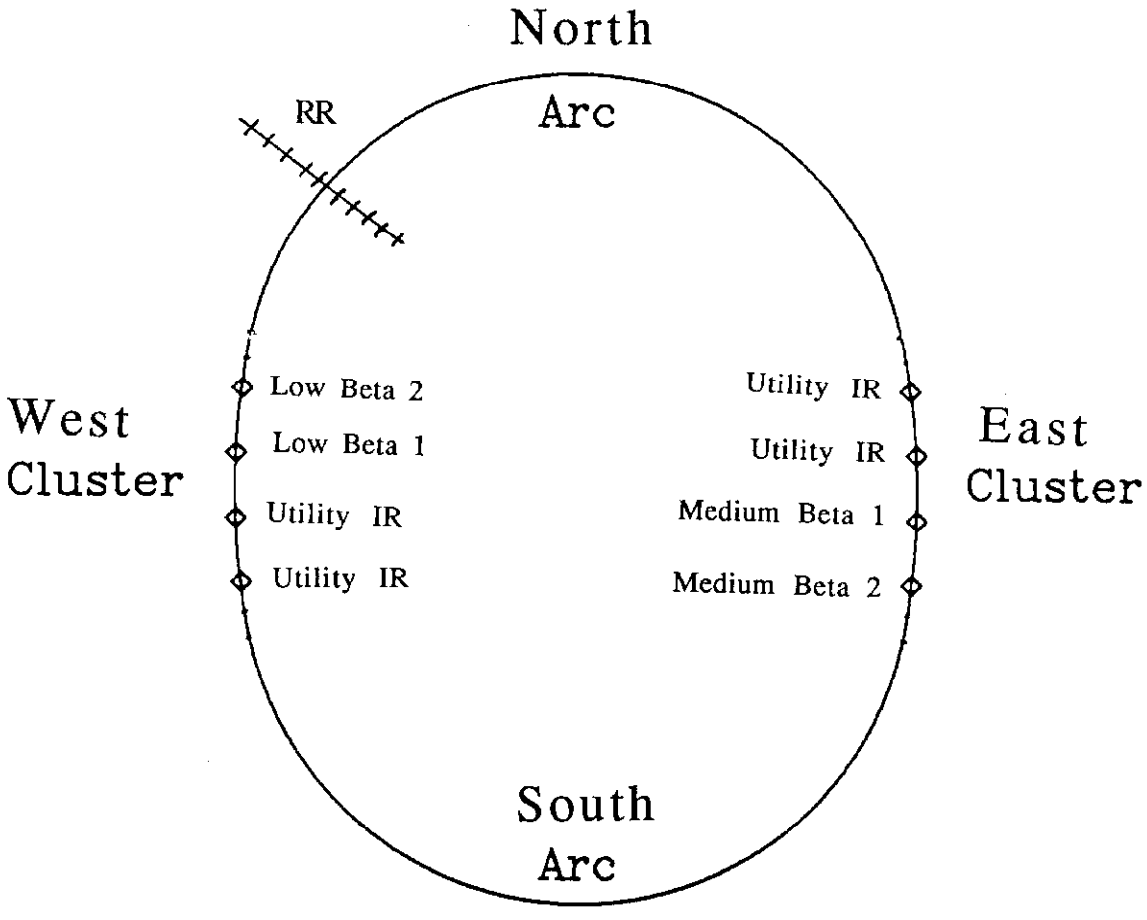

Fig. 7. Layout of the SSC ring.

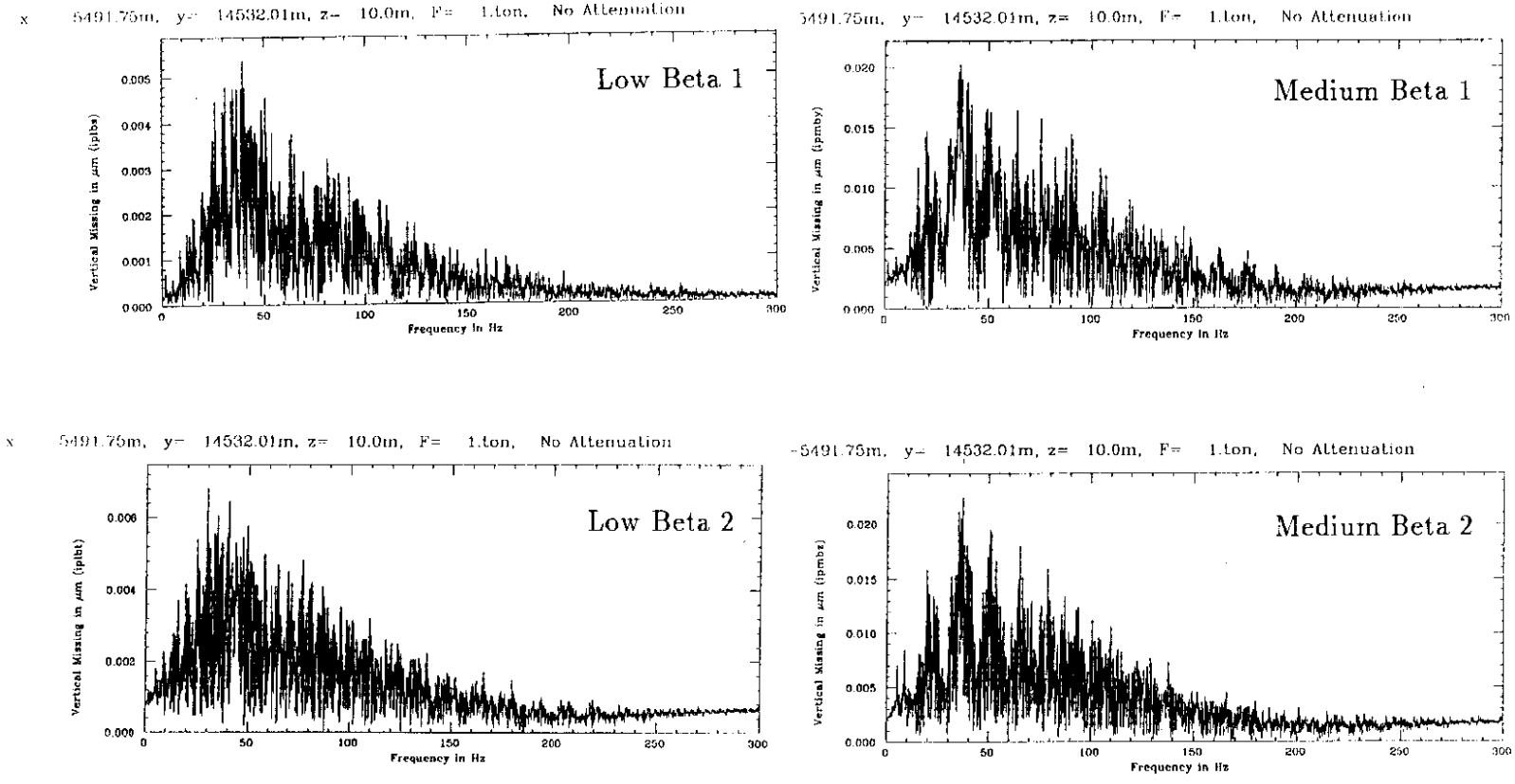

Fig. 8a. The spectrum of the vertical beam separation at the four interaction points due to ground waves from a vibrating source located on the surface in the northwest region of the northern arc where the South Pacific Railroad crosses over the SSC ring. The source is a 1-ton vertical force at each frequency. The tunnel depth is taken as 10 meters and uniform. No attenuation due to absorption was assumed.

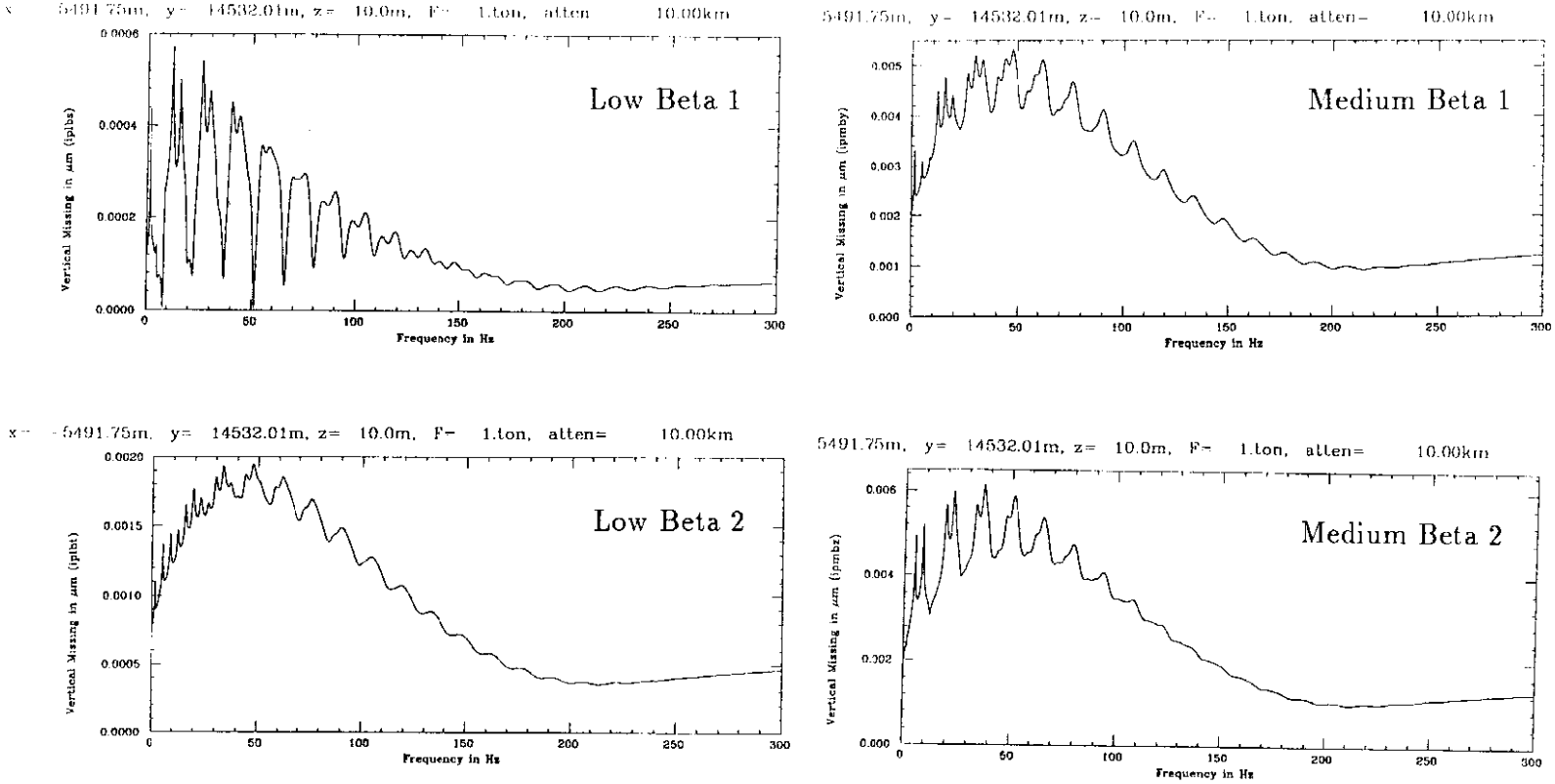

Fig. 8b. The spectrum of the vertical beam separation at the four interaction points, as in Figure 8a, but with a characteristic absorption length of 10 km (at 1 Hz).

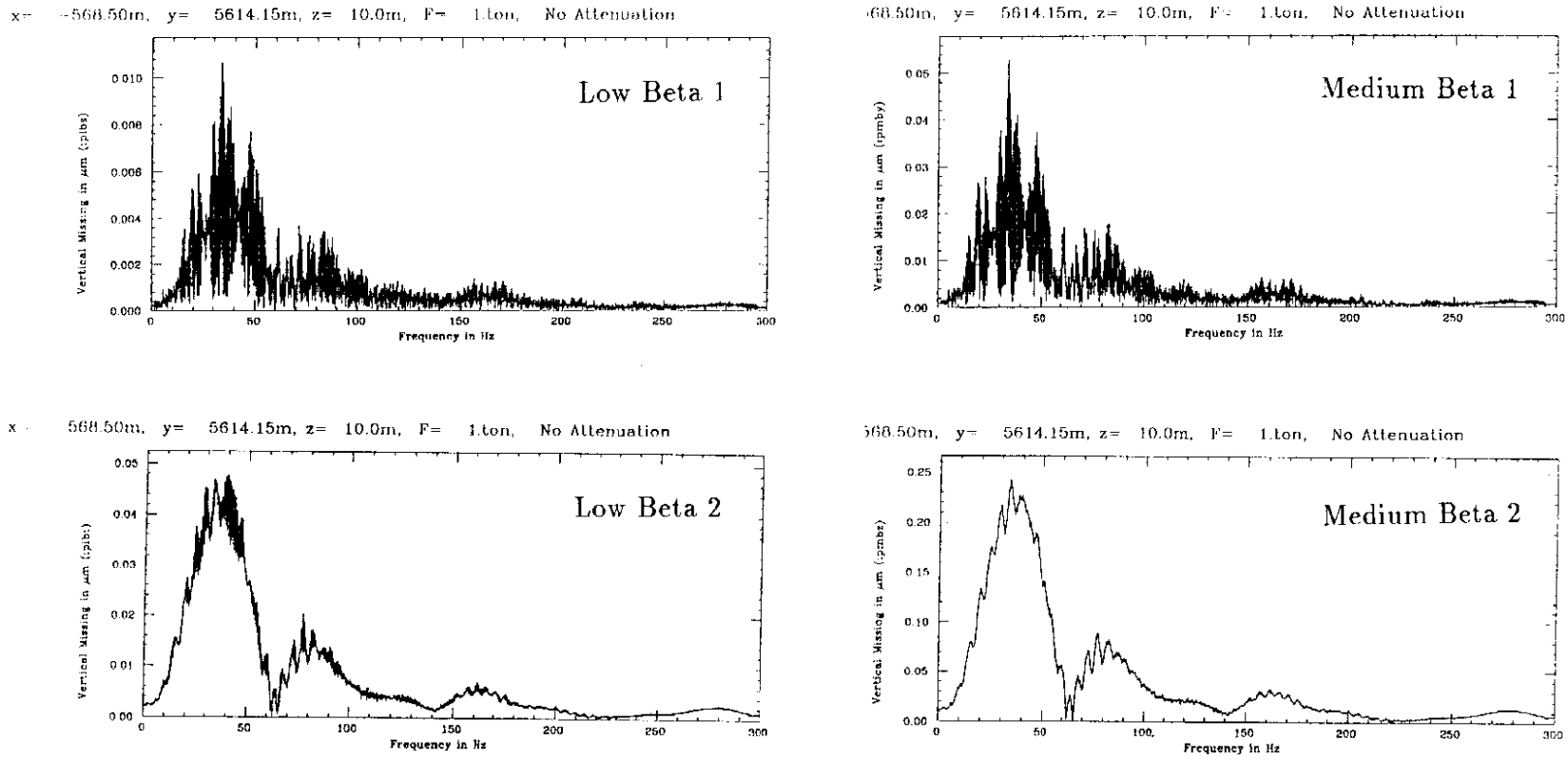

Fig. 9. The spectrum of the vertical beam separation at the four interaction points when the 1-ton vibrating force is directly over the Low-Beta-1 interaction point.

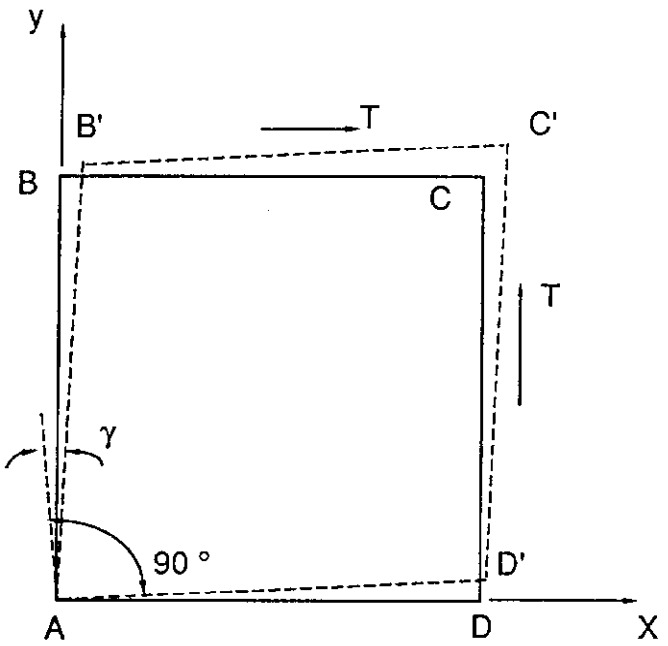

Fig. 10. A body distorted by pure shear stress T.

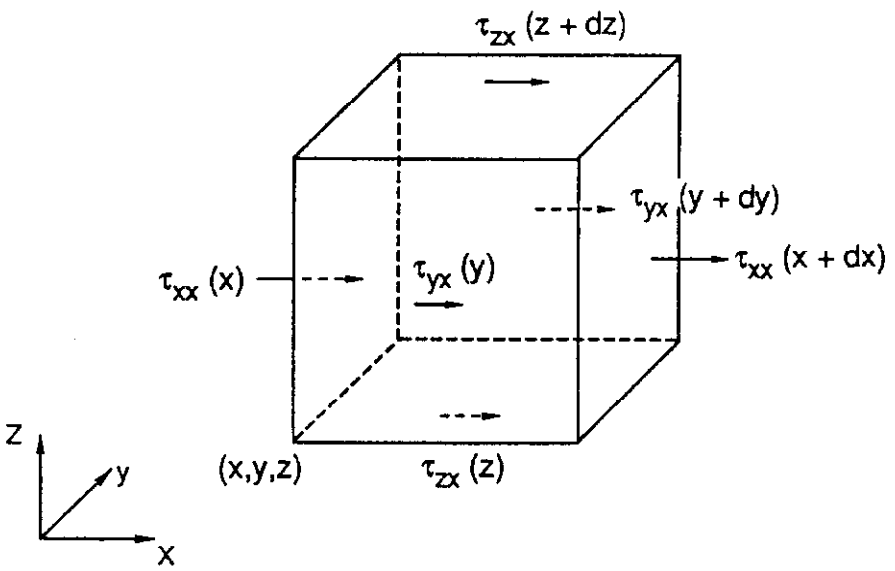

Fig. 11. The force in the x-direction due to stresses on the six surfaces of a cubic element.

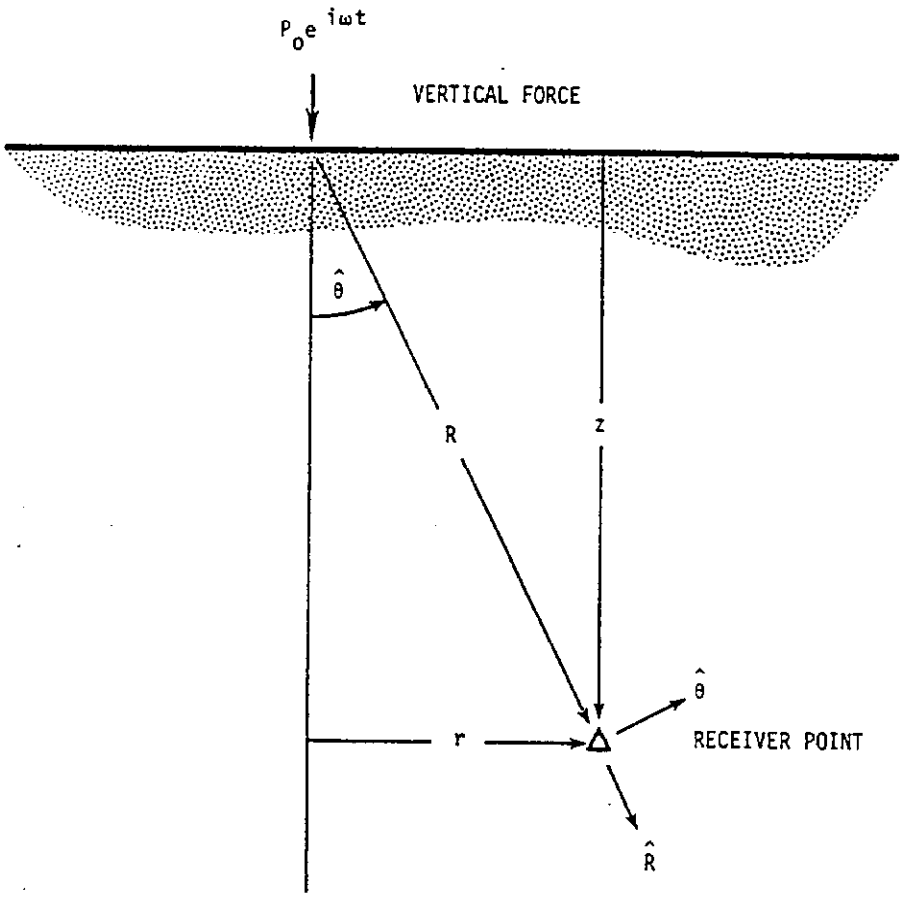

Fig. 12. Vertical point load on surface of elastic half-space.